Forces on Jacket Structures: Effects of Directionality and Spectral Shapes

by

Ong Zhen Liang

17000570

Dissertation submitted in partial
fulfilment of the requirements for the
Bachelor of Engineering
(Hons) (Civil)

JANUARY 2021

Universiti Teknologi
PETRONAS Bandar Seri
Iskandar
31750 Tronoh
Perak Darul Ridzuan

CERTIFICATION OF APPROVAL

Forces on Jacket Structures: Effects of Directionality and Spectral Shapes

by

Ong Zhen Liang
17000570

A project dissertation submitted to the
Civil Engineering Programme
Universiti Teknologi PETRONAS
in partial fulfilment of the requirement for the
BACHELOR OFF ENGINEERING (Hons)
(CIVIL)

Approved by,

(Dr Mohamed Latheef)

UNIVERSITI TEKNOLOGI PETRONAS
TRONOH, PERAK

Jan 2021

CERTIFICATION OF ORIGINALITY

This is to certify that I am responsible for the work submitted in this project, that the original work is my own except as specified in the references and acknowledgements, and that the original work contained herein have not been undertaken or done by unspecified sources or person.

(ONG ZHEN LIANG)

ABSTRACT

In Malaysia, the majority of oil platforms are comprised of jacket structures. Despite reassessments having been conducted regularly, existing jacket structures might be subjected to conditions more critical than ever due to numerous reasons which include the plan of utilizing the existing structures beyond its design life. Furthermore, the existing structures are only designed to withstand regular wave loadings without considering other load cases which raises even more concerns about the structural integrity. Hence, this work aims to assess the structure under irregular wave loadings, compare the loadings on the structure under the effects of directionality and different spectral shapes. The research methodology is divided into three main stages. The first stage is to develop the code, followed by the second stage, where wave loadings under the effects of directionality and different spectral shapes are calculated, and the last stage is to compare the forces obtained from the code with the old method. The total substructure load was computed from regular waves based on Stokes' 5^{th} Order Wave Theory and irregular waves represented by two different spectral shapes, which were JONSWAP spectrum and the observed spectral shape in Southern South China Sea (JONSWAP-Swell), based on 2^{nd} Order Random Wave Theory. The load from irregular waves showed only slightly higher magnitudes in comparison to regular waves, with JONSWAP achieving an even higher magnitude compared to JONSWAP-Swell. However, above still water level, the force generated by JONSWAP is significantly higher than both JONSWAP-Swell and regular waves, where JONSWAP-Swell yields a slightly higher force than regular waves. When both spectral shapes were directionally spread over 15^{o}, the change in the total horizontal substructure forces in both spectral shapes is rather insignificant. However, when the degree of directionality was increased to 30^{o}, both spectral shapes observed a reduction of 10% to 15% in the total horizontal substructure force.

ACKNOWLEDGEMENT

I am eternally grateful for Dr. Mohamed Latheef for giving me an opportunity to become one of his Final Year Project students. Throughout this project, Dr Latheef has been providing me with all the guidance I needed to get on with this project. He answered my questions tirelessly to make sure I understand everything fully. His passion towards this topic and his patience towards my endless questions have fueled my motivation to complete this project with my best effort. It is my honour to have Dr Latheef as my supervisor for my Final Year Project.

I would wish to express my sincere gratitude for all the support I received from my family when I was working on this project. They made sure to try their best to create a conducive learning environment at home during this online semester. I can never thank my parents enough for being so supportive when I chose to study Civil Engineering in Universiti Teknologi PETRONAS.

Additionally, I wish to thank my fellow friends, Fong, William, Koay, Ahmed, Arinah and many others for generously sharing their knowledge and experience regarding this topic so that I can have a better understanding in my FYP topic. Also, many thanks to Alex, Peter, Kah Wai and Sze Kuan, whom I befriended since the first day I joined this university, for making my experience in UTP a fun one. All the best in life.

Last but not least, I would like to thank my SAS advisor, Dr Husna, for being such a caring advisor throughout my studies in UTP. Be it academic or non-academic matters, she always listened to our problems and offered us her wise advices.

TABLE OF CONTENTS

LIST OF FIGURES

LIST OF TABLES

1. INTRODUCTION

1.1. Background of Study

In places where hydrocarbon reserves are found in Malaysia, the water depths at these locations can be categorized as shallow water. Owing to the relatively shallow water depth, the majority of the structures used in the recovery process of petroleum are fixed offshore structures such as jacket structures. Jacket structures are widely employed compared to other fixed offshore structures because it simply functions best in such water depths, thus making it the most economical option there is. Existing jacket structures, despite having been designed for a long return period, will still have to undergo reassessment within regular periods of time to ensure its operational reliability.

In Malaysia where the wind loading is relatively milder, the main lateral load component acting on jacket structures is wave loading. Most of the jacket structures in Malaysia are designed to withstand the wave loading of a regular wave or at best included up to a linear contribution. To add to the complication, in real sea, waves are not unidirectional as different wave components travels in different angles and these waves are often non-linear waves. In multi-directional waves, the height varies along the length, therefore resulting in the formation of short-crested waves. This phenomenon is known as wave directionality.

Other than wave directionality, spectral shape of waves also plays a huge role in determining the wave loading on jacket structures. Among the wider-known spectral shapes, JONSWAP spectrum is the most widely used spectral shape in calculations. However, JONSWAP spectrum is based on the spectral shape observed in North Sea, while oil platforms in Malaysia are located in Southern South China Sea. This means that JONSWAP spectrum is not reflective of the sea state in Southern South China Sea. To maximise the accuracy of the calculation during the design process, it is recommended that the spectral shape of waves observed in Southern South China Sea is used rather than JONSWAP spectrum.

1.2. Problem Statement

There are several issues arising for existing jacket structures in Malaysia. The first issue involves the design of existing jacket structures which only incudes regular wave loading as the main lateral load component. While this practice simplifies the situation for easier analysis and design process, the negligence of wave phenomena such as non-linearity and directionality can result in errors in the design of jacket structures. If said wave phenomena were included in the calculation, some parts of the structures may be overdesigned or under-designed. In addition to the first problem, most platforms are designed based on the more popular JONSWAP spectrum which is not reflective of the sea state in Southern South China Sea, thus introducing more errors to the design.

1.3. Objectives

Given the issues mentioned in Problem Statement, the following are the objectives of this study:

- To assess the loading on jacket structures by considering the effects of wave directionality
- To check the loads on jacket structures under nonlinear random waves loading with the effects of wave directionality and compare them against different spectral shapes

Scope of Study

This study will focus on computing the loads on jacket structures under the combined effects of loading conditions mentioned in above objectives. The loadings considered on the structure are only static loadings while the structure under consideration is a fixed structure. The computation of loads is also only limited to using analytical wave theory and no numerical methods will be implemented.

2. LITERATURE REVIEW

2.1. Wave Forces – Morison's Equation

Morison's Equation (Morison et al., 1950) expressed below is used to calculate the force per unit length acting on a tubular member,

$$f_T = \rho C_M A \frac{\partial u}{\partial t} + \frac{1}{2}\rho C_D D u|u| \qquad \text{(Eq. 2.1)}$$

where ρ is the fluid density, taken is 1025 kg/m^3, A is the cross-sectional area of the tubular member, D is the diameter of the member, C_D and C_M are the drag coefficient and coefficient of inertia respectively, u is the normal component of the water particle kinematics and $\frac{\partial u}{\partial t}$ is the normal component of the fluid acceleration.

Morison's equation contains two terms that describe the total force acting on the structure's substructure. The first term is the inertia force and it depends on the acceleration of water particles due to the $\frac{\partial u}{\partial t}$ component in said term. The second term describes the drag force acting on the member. It varies quadratically with the velocity. Morison et al. (1950) described the horizontal water particle kinematics, u, with linear wave theory as shown in Equation 2.2 while the acceleration of water particles is described in Equation 2.3.

$$u = \frac{a\omega \cosh(kz) \sin(\omega t - kx)}{\sin h(kd)} \qquad \text{(Eq. 2.2)}$$

where a is the amplitude of the wave, ω is the wave frequency, k is the wave number, z is the distance from the seabed to the crest elevation and d is the depth of water level.

$$\frac{\partial u}{\partial t} = \frac{a\omega^2 \cosh(kz) \cos(\omega t - kx)}{\sin h(kd)} \qquad \text{(Eq. 2.3)}$$

However, due to the insufficient accuracy from the incorporation of linear wave into the structure's design, a number of other methods were developed to compute the water particle kinematics but according to Latheef et al. (2018), Stokes' 5th order solution is the most widely used method. Stokes' 5th order solution is an

analytical solution which makes it relatively easier to be implemented but its accuracy of prediction is only limited to regular wave models.

The Stokes' 5th order solution describes the horizontal water particle kinematics in Equation 2.4 (Fenton, 1985).

$$u = C_0 \left(\frac{g}{k^3}\right)^{\frac{1}{2}} \sum_{i=1}^{5} \sum_{j=1}^{i} \in^i A_{ij} cosh(jk(z+d)) sin(j(kx-\omega t)) \qquad \text{(Eq. 2.4)}$$

where $\varepsilon = {}^{kH}/_{2}$, g is the gravitational acceleration while A_{ij} and C_i are functions of wave number, k and water depth, d provided by Fenton (1985).

Despite regular waves being less representative of the real sea state compared to irregular waves, most designs still adopt Stokes' 5th order solution because it is assumed that this method provides a more conservative analysis by using a regular wave of the largest wave height from the data recorded at sea. However, Swan et al. (2016) has proven this assumption to be only partially correct by making a comparison between the water particle kinematics as predicted by various wave models and the water particle kinematics of experimental data. This comparison is shown in Figure 2.1 where the water particle kinematics of a non-breaking wave at different elevations are plotted.

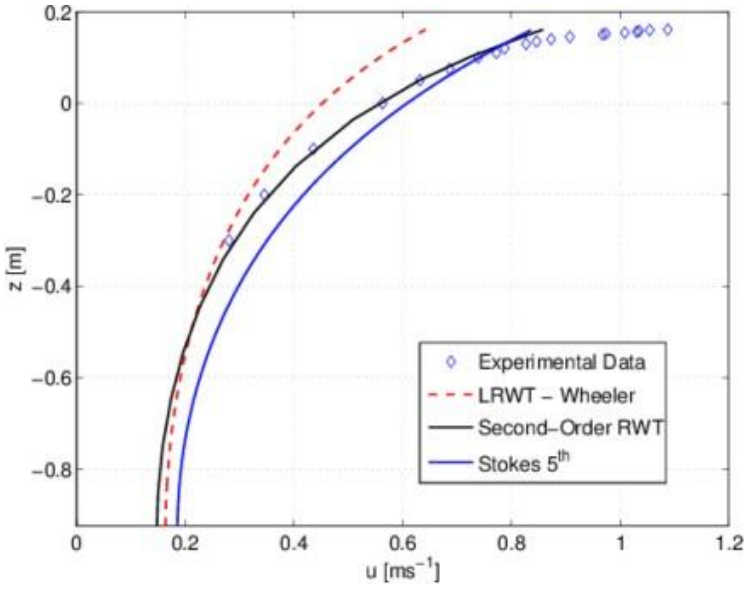

Figure 2.1: Water particle kinematics of different wave model predictions and experimental data (non- breaking wave) (Swan et al., 2016)

In Figure 2.1, it shows that at the substructure level, Stokes' 5th order solution predicts a higher fluid velocity compared to experimental data. This means that at the substructure level, the design based on Stokes' 5th order solution will be more conservative but this does not necessarily mean it is a good approach as overdesigning can raise economical issues in future projects. On the contrary, at the superstructure level, Stokes' 5th order solution predicts lower velocity than the experimental data suggests. This means troubles for existing structures as it indicates that the superstructure designed using Stokes' 5th order solution is under-designed.

2.2. Nonlinearity

In a random sea state consisting of a large number (M >> 1) of *linear free waves*, the linear summation of all wave components gives:

$$\eta = \sum_{m=1}^{M} a_m cos(k_m x - \omega_m t + \alpha_m) \qquad \text{(Eq. 2.5)}$$

$$u = \sum_{m=1}^{M} a_m \omega_m \frac{cosh k_m (z+d)}{sinh(k_m d)} cos(k_m x - \omega_m t + \alpha_m) \qquad \text{(Eq. 2.6)}$$

where $\omega_m^2 = g k_m \tanh(k_m d)$

However, in practice not all the wave components are linear free waves. In fact, many of them are bound waves and they are nonlinear. For example, when two freely propagating wave components of different wavelengths interact with each other, linear wave theory gives the solution from the interaction of the two wave components as the simple summation. But if we incorporate nonlinearity into the problem, the velocity of the resultant wave at $z = \hat{z}$ would be:

$$u = a_1\omega_1 \frac{\cosh k_1(z+d)}{\sinh(k_1 d)} \cos(k_1 x + \omega_1 t) + a_2\omega_2 \frac{\cosh k_2(z+d)}{\sinh(k_2 d)} \cos(k_2 x + \omega_2 t) \qquad \text{(Eq. 2.7)}$$

Unfortunately, this solution will produce large errors due to the extrapolation of short-wave velocities to $z = \hat{z}$ where $\hat{z} \gg a_2$ and depends on the amplitude of the

long wave (a_1). This is usually referred to as *high-frequency contamination*, which causes significant over-prediction of horizontal velocity beneath the wave crest.

2.3. Wave Directionality

Linear representation of unidirectional waves within a wavefield is given as,

$$\eta = \sum_{m=1}^{M} a_m co\ s(\omega_m t - k_m x + \alpha_m) \qquad \text{(Eq. 2.8)}$$

where a_m is the random phase (lying between 0 to 2π) for the m^{th} wave component and x defines the direction of wave propagation. However, in real seas, some wave components travel at an angle θ to the mean wave direction. If directionality is incorporated in design, it is a common practice to assume that the directional and frequency distribution are independent. A spectral representation therefore assumes,

$$S_{\eta\eta}(\omega, \theta) = D(\theta) S_{\eta\eta}(\omega) \qquad \text{(Eq. 2.9)}$$

where $S_{\eta\eta}(\omega)$ is the frequency distribution function, and $D(\theta)$ is the directional distribution function.

According to Eq. 2.9, the same directional distribution applies to all frequency components. This is incorrect since swell waves have small directional spread, effectively making swell waves unidirectional, while wind waves may have a large directional spread. Unfortunately, since there is no clear procedure to separate swell waves and wind waves as of now, applying a generalized directional spread is the best option. Therefore, for design purposes, directionality is usually represented by either:

i. A normal distribution:

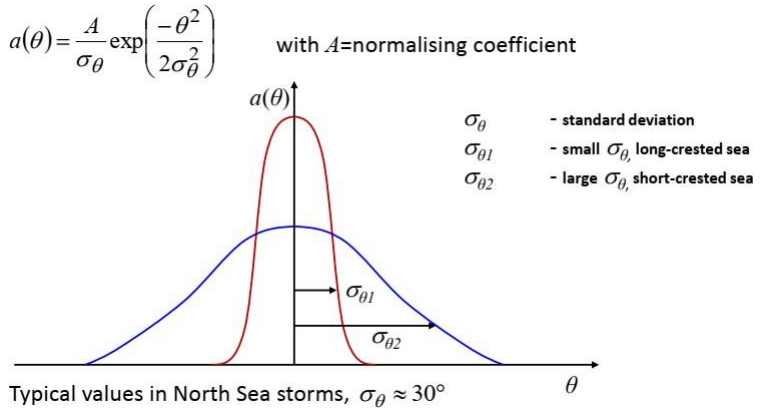

Figure 2.2: Normalised wave amplitude distribution due to directional spreading

ii. Mitsuyasu distribution

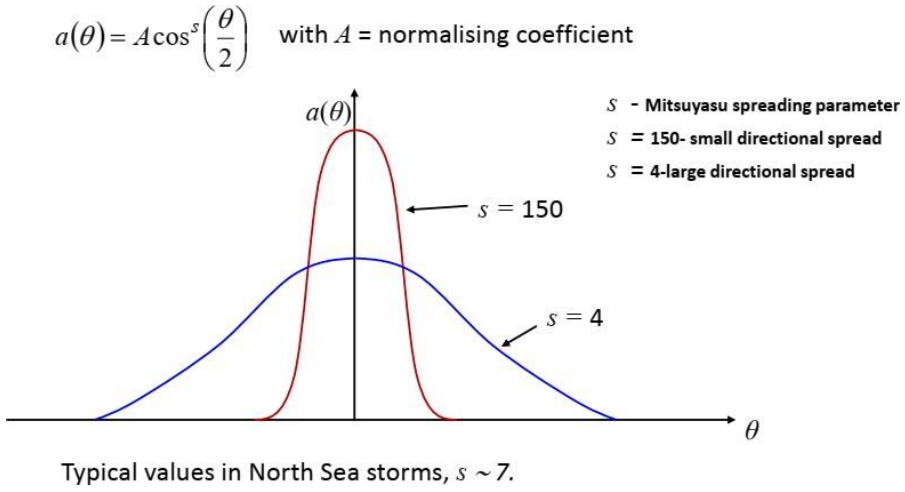

Figure 2.3: Mitsuyasu distribution of wave amplitude due to directional spreading (Mitsuyasu et al., 1975)

Surface Elevation

From a linear perspective, directionality makes no difference to the maximum crest elevation. On the other hand, from a nonlinear perspective, it does because of changes to the wave slope.

Linear solution for directionally spread waves gives:

$$\eta(x, y, t) = \sum_{freq.} \sum_{dir.} a_m cos\,(\omega\, t_m - k^{(x)}_m x - k^{(z)}_m z + \alpha\,)_m \qquad \text{(Eq. 2.10)}$$

where $k^{(x)}_m x$ – wave number in *x*-direction for the m^{th} component.

$k^{(z)}_m z$ – wave number in *z*-direction for the m^{th} component.

In unidirectional waves, the wave height is constant along the length, resulting in long-crested waves, whereas in multi-directional waves, the weight height varies along the length, creating short-crested waves. The greater the directionality, the more short-crested the individual waves are. This suggests that directionality is important since jacket structures have a large spatial dimension.

Water Particle Kinematics

The water particles kinematics beneath a large wave are always affected by directionality. The linear solution of water particle kinematics under the effects of directionality gives:

$$u = \sum_{freq.} \sum_{dir.} a_m \omega_m \frac{coshk_m(z+d)}{sinh(kd)}\, cos(\omega_m t - k^{(x)}_m x - k^{(z)}_m z + \alpha_m) \qquad \text{(Eq. 2.11)}$$

where $k^2_m = [(k^{(x)}_m)^2 + (k^{(z)}_m)^2]$

As discussed earlier that many problems arise with applying linear random wave theory to unidirectional waves, similar problems exist in multi-directional waves, particularly high-frequency contamination. There are a few ways to overcome this difficulty:

a) Apply a directional second-order random wave model, which is the extension of original work proposed by Longuet-Higgins & Steward
b) Adopt a fully nonlinear directional wave model as proposed by Bateman, Swan & and Taylor (2001)
c) Apply a *Velocity Reduction Factor* (typically ranging from 0.8 to 0.9, depending on $\sigma_\theta$or *s)* to the calculation of unidirectional velocities in order to account for average directional spread

d) Design based on unidirectional waves, which is acceptable for fixed structures but not acceptable for floating structures.

2.4. Spectral Shapes

JONSWAP is the most commonly used sea spectrum to model a typical wind sea (Latheef, 2014). This empirical spectrum was derived as a best fit to observed wind and wave data from the North Sea. The spectral density function for this sea state is

$$S_{w,\eta\eta}(\omega) = \frac{(2\pi)^4 \alpha g^2}{\omega^5} exp\left[-\beta \frac{\omega_p^4}{\omega^4}\right] \gamma^{exp\frac{-(\omega-\omega_p)^2}{2\omega_p^2\sigma^2}} \quad \text{(Eq. 2.12)}$$

where ω_p is the circular wave frequency corresponding to the spectral peak period T_p, γ is the peak enhancement factor, α is the Phillips' parameter, $\beta = 1.25$, $\sigma = 0.07$ for $\omega \leq \omega_p$ and 0.09 for $\omega > \omega_p$. Subscript '*w'* is appended to symbol '*S'* to indicate that this function corresponds to a wind sea state.

However, in Southern South China Sea, the most severe sea states in this region contain mostly swell (Latheef et al., 2020). One of the popular choices for the representation of the swell component is a Gaussian shape expressed as

$$S_{s,\eta\eta}(\omega) = \left[\frac{(0.25H_s)^2}{\sigma\sqrt{2\pi}}\right] \exp\left[\frac{-(\omega-\omega_p)^2}{2\sigma^2}\right] \quad \text{(Eq. 2.13)}$$

where σ is the standard deviation of the resulting Gaussian spectrum. Subscript *'s'* is appended to symbol '*S'* to indicate that this is the corresponding spectral density function of a swell sea.

For mixed seas with both a wind and a swell component, the spectral density function is expressed as a linear superposition of the wind and swell components

$$S_{\eta\eta}(\omega) = S_{w,\eta\eta} + S_{s,\eta\eta} \quad \text{(Eq. 2.14)}$$

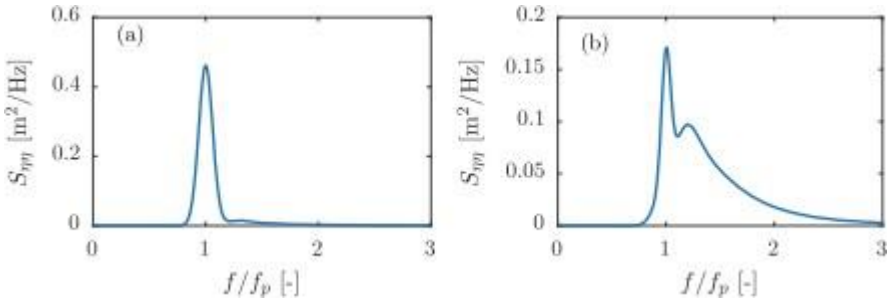

Figure 2.4: Generalised spectra for a L1 and b L2 after considering the spectral parameters obtained from 5 largest storms for H_s=1m. (Latheef et al., 2020)

In order to incorporate spectral shapes and wave directionality into the computation of wave forces, wave particle kinematics is needed, which can be obtained from the spectral density function defined in Eq. 2.14 and the directional spreading function described below in Eq. 2.15.

$$D(f,\theta) = \frac{1}{\pi}\{\frac{1}{2} + \sum_{n=1}^{\infty}[A_n(f)cos\, n\theta + B_n(f)sin\, n\theta]\} \qquad \text{(Eq. 2.15)}$$

where $A_n(f)$ and $B_n(f)$ are the Fourier coefficients and θ is the mean wave direction.

With both spectral density function and the directional spreading function defined, the frequency power spectrum can then be described as

$$F(f,\theta) = S_{\eta\eta}(f)D(f,\theta) \qquad \text{(Eq. 2.16)}$$

From the frequency power spectrum described in Eq 2.16, the wave amplitude can be calculated using Eq. 2.17 and the velocity function can then be obtained using the computed wave amplitude as described in Eq. 2.18

$$a(\omega,\theta) = \sqrt{2F(\omega,\theta)d\omega d\theta} \qquad \text{(Eq. 2.17)}$$

$$\phi = \sum_{i=1}^{\infty} b_i \frac{cosh[k_i(d+z)]}{cosh[k_i\, d]} sin(\psi_i) \qquad \text{(Eq. 2.18)}$$

where $b_i = \frac{a_i g}{w_i}$, and $\psi = k_i \cdot x - \omega_i t + \psi_i$, k is the wave number. The derivative of Eq 2.18 with respect to x gives the horizontal water particle kinematics of irregular waves. However, this is only a simple linear summation with the assumption of no interaction between wave components. Therefore, a second-order correction is applied to the linear solution as proposed by Longuet-Higgins & Stewart (1960) which is then generalized by Sharma & Dean (1981) as follows

$$\phi^{(2)} = \frac{1}{4}\sum_{i=1}^{\infty}\sum_{j=1}^{\infty} b_i b_j \frac{cosh k_{ij}^{-}(d+z)}{cosh k_{ij}^{+} d} \frac{D_{ij}^{-}}{\omega_i - \omega_j} sin(\psi_i - \psi_j) + \frac{1}{4}\sum_{i=1}^{\infty}\sum_{j=1}^{\infty} b_i b_j \frac{cosh k_{ij}^{+}(d+z)}{cosh k_{ij}^{+} d} \frac{D_{ij}^{+}}{\omega_i - \omega_j} sin(\psi_i + \psi_j) \quad \text{(Eq. 2.19)}$$

with

$$k_{ij}^{-} = |k_i - k_j| \qquad k_{ij}^{+} = |k_i + k_j| \quad \text{(Eq. 2.20)}$$

$$D_{ij}^{+} = \frac{(\sqrt{R_i} + \sqrt{R_j})[\sqrt{R_i}(k_j^2 - R_j^2) + \sqrt{R_j}(k_i^2 - R_i^2)]}{(\sqrt{R_i} + \sqrt{R_j})^2 - k_{ij}^{+}\tanh(k_{ij}^{+} d)} + \frac{2(\sqrt{R_i} + \sqrt{R_j})^2 (k_i \cdot k_j - R_i R_j)}{(\sqrt{R_i} - \sqrt{R_j})^2 - k_{ij}^{+}\tanh(k_{ij}^{+} d)} \quad \text{(Eq. 2.21)}$$

$$D_{ij}^{-} = \frac{(\sqrt{R_i} - \sqrt{R_j})[\sqrt{R_j}(k_i^2 - R_i^2) - \sqrt{R_i}(k_j^2 - R_j^2)]}{(\sqrt{R_i} + \sqrt{R_j})^2 - k_{ij}^{-}\tanh(k_{ij}^{-} d)} + \frac{2(\sqrt{R_i} - \sqrt{R_j})^2 (k_i \cdot k_j + R_i R_j)}{(\sqrt{R_i} - \sqrt{R_j})^2 - k_{ij}^{-}\tanh(k_{ij}^{-} d)} \quad \text{(Eq. 2.22)}$$

$$R_i = k_i \tanh(k_i d) \quad \text{(Eq. 2.23)}$$

This allows the incorporation of spectral shapes into Morison's Equation for the calculation of wave forces.

3. METHODOLOGY

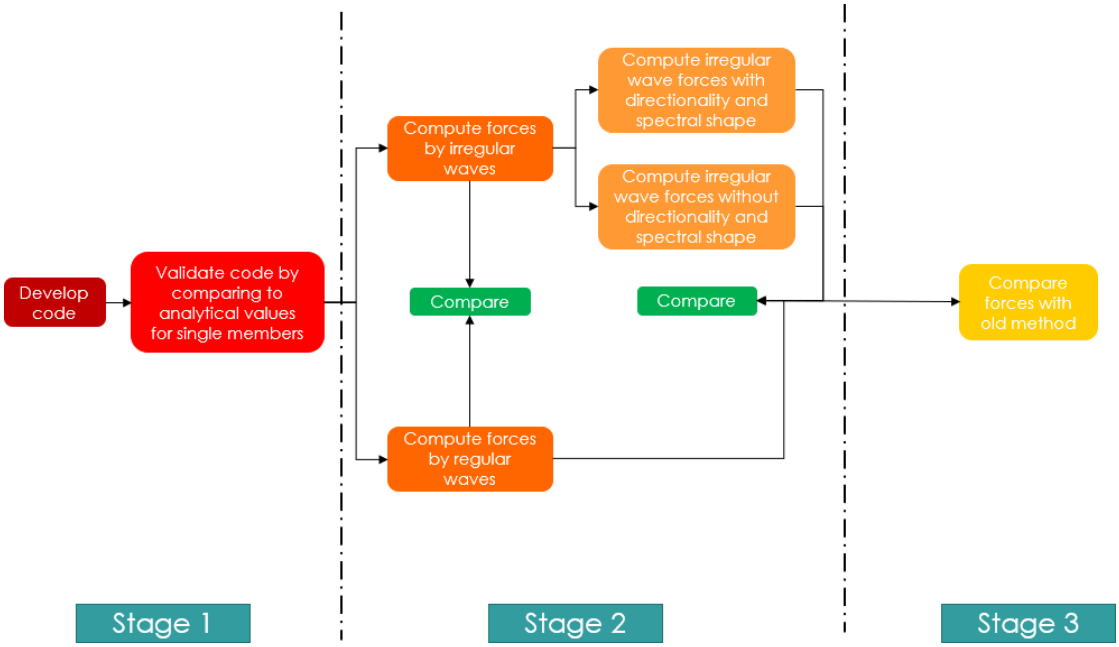

Figure 3.1: Research methodology

Stage 1

In Stage 1, a MATLAB code is developed to model the jacket structure. The code is based on Morison's Equation (Eq. 2.1) for the computation of forces acting on the structures. In this stage, only static loading is considered. This means that the structure is not dynamically reacting to the forces from waves. Upon the development of the MATLAB code, the code is validated by comparing the results against the analytical values calculated from Linear Airy Wave Theory (described in Eq. 2.2 and Eq. 2.3) for single members and the code is further refined if there is any error.

Stage 2

The code is further developed to compute loadings on the structure from waves with and without the effects of directionality and different spectral shapes based the code developed in Stage 1. The different waves that will be used include regular waves up to 5th order and nonlinear random wave up to 2nd order provided by Longuet-Higgins & Stewart (1960) described in Eq. 2.19 to Eq. 2.23. Two different spectral shapes will

be used for the comparison, which are JONSWAP spectrum and the observed spectrum in Southern South China Sea as proposed by Latheef et al. (2020).

Stage 3

In Stage 3, the forces under the effects of directionality and spectral shapes due to different wave theories obtained from Stage 2 are compared against each other and with the old method.

Jacket Structure Model and Loading Criteria

The jacket structure is composed of multiple cylindrical members each having diameter of 1m. The structure consists of four vertical legs that are 10m apart and are braced with horizontal and diagonal members of 0.5m diameter at every 10m height at all four faces. A 3D view of the jacket structure legs and bracings is attached in the appendix (Appendix 1). The substructure legs and bracings were loaded with horizontal forces generated using a force model built upon Morison's Equation described in Equation 2.1. A group of regular waves approximated based on Stokes' 5^{th} Order Wave Theory was used as a reference during the computation of total horizontal substructure force for the comparison against irregular waves approximated based on 2^{nd} Order Random Wave Theory under the effects of different spectral shapes and directionality. Two different spectral shapes were adopted to examine the effect of spectral shapes on the total horizontal substructure force. These spectral shapes are JONSWAP spectrum and the observed spectral shape in Southern SCS. Directionality was only incorporated in irregular waves of the above-mentioned spectral shapes as Stokes' 5^{th} Order Wave Theory is only applicable in regular waves.

Verification of MATLAB Code

To ensure the accuracy of the results produced from the code developed to model the jacket structure and apply the force model, the results were verified against manual calculations. For verification purposes, one single column was inserted into the MATLAB code and the column was simulated with linear regular wave condition for easier manual calculations. This column was placed in three different coordinates to simulate three different conditions. The first column (C1) was placed at wave trough,

the second column (C2) was placed at wave crest and the third column (C3) was placed at wave crest but was fully submerged below the water. Table 3.1 shows the force magnitudes obtained from manual calculations for C1, C2 and C3. The detailed step-by-step manual calculations are attached in Appendix 2. Figure 3.2 shows the force of each column produced using the developed code. By comparing the values from Table 3.1 with the values observed in Figure 3.2, a slight difference in the values can be observed. This slight difference is caused by rounding off the intermediate values to the second or third decimal place when manual calculations were performed. On the other hand, MATLAB is able to store intermediate values with higher precision without rounding off, causing the values obtained from the code to be slightly different. However, the similarity between the values obtained from manual calculations and MATLAB code provides the evidence that the code is indeed working as intended.

Table 3.1: Summary of forces for each column from manual calculations

Column	**C1**	**C2**	**C3**
Forces (N)	9.5791×10^4	2.4812×10^5	4.5017×10^4

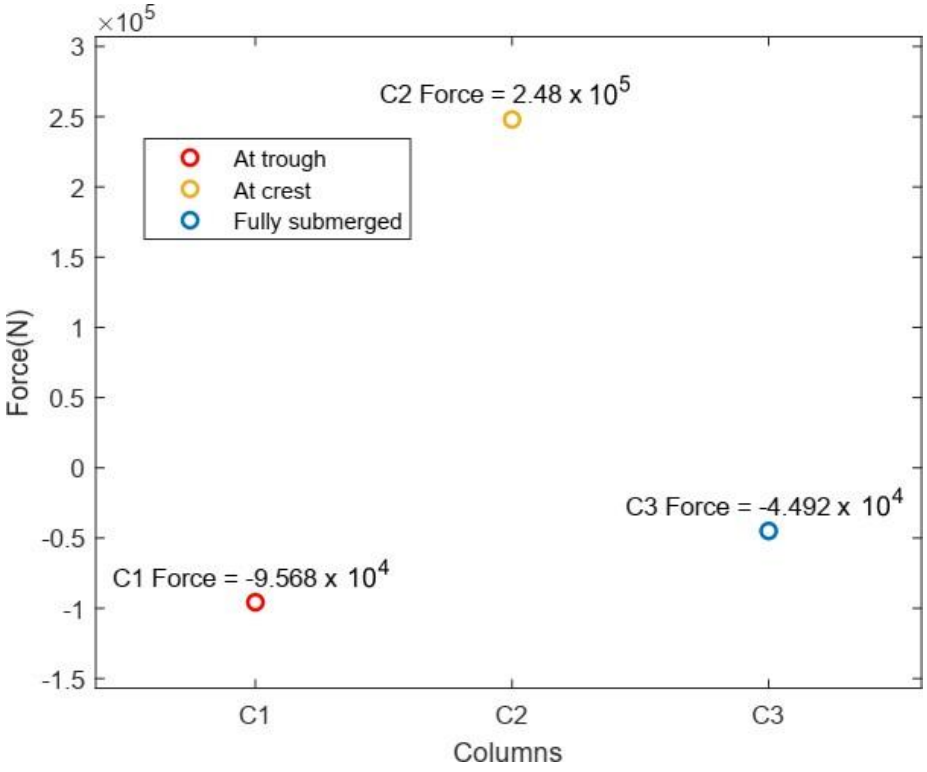

Figure 3.2: Force magnitude of columns computed by code.

Time Range of Directional Cases

To study the effect of directionality on the total horizontal substructure force, the individual wave components were spread normally by Gaussian Distribution. By doing so, the code would need to loop through more than 2000 wave components for each time instant in each member of the structure. The process can be very time consuming if the time range was set to a similar length as that of the unidirectional cases. Fortunately, from the total horizontal force-time history of the unidirectional cases, the time instant when the maximum total horizontal force occurred can be determined. For both spectral shapes, the maximum total horizontal forces occurred within the time range of -0.5s to 0.5s. Due to the time constraint and the limited computing power available, the time range for directional cases were set from -0.5s to 0.5s to obtain only the maximum total horizontal forces for both spectral shapes.

4. RESULTS AND DISCUSSION

The code was developed to model a jacket structure which was subjected to wave loading by either regular waves or irregular waves with zero current. For regular waves, the force computation was based on Stokes' 5th Order Wave Theory as it is the most widely adopted wave theory in the industries. In real seas where the waves are steep in nature, linear wave theory can no longer be used to predict the waves accurately as it only works on small amplitude waves. Stokes' 5th, on the other hand, can predict the waves with a higher order of accuracy as it includes the higher order term omitted by linear wave theory. Since it has been the industries' preferred analysis theory, the value of total horizontal substructure force from regular waves based on Stokes' 5th serves great as a reference for the comparison against other cases included in this study. For irregular waves, 2nd Order Random Wave Theory was adopted as it eliminates the *high frequency contamination*, which plagues the Linear Random Wave Theory and results in extremely large forces as discussed in Chapter 2. Two different spectral shapes were chosen for examining the effect of spectral shapes on the total horizontal force. These spectral shapes are JONSWAP and the observed spectral shape in Southern South China Sea, which will be referred to as JONSWAP-Swell. JONSWAP spectrum was adopted because it is one of the most used spectral shape in the design of offshore platforms, therefore it serves as a reference value for irregular waves. For a more accurate representation of the sea state in Malaysia, JONSWAP-Swell was used as the spectrum is specifically fitted to the observed spectral shape in Southern South China Sea. To ensure a fair comparison, the regular waves and each spectral shape representing irregular waves were configured to have the same wave height (Hs). Specific to JONSWAP spectrum, the peak period was set to have the same value as regular waves. Meanwhile, the swell component in JONSWAP-Swell has a different peak period while the wind component, which is represented by JONSWAP, also has a peak period of the same value as regular waves. Figure 4.2.1 below shows the comparison of the total horizontal force-time history between different types of waves and their respective wave theory.

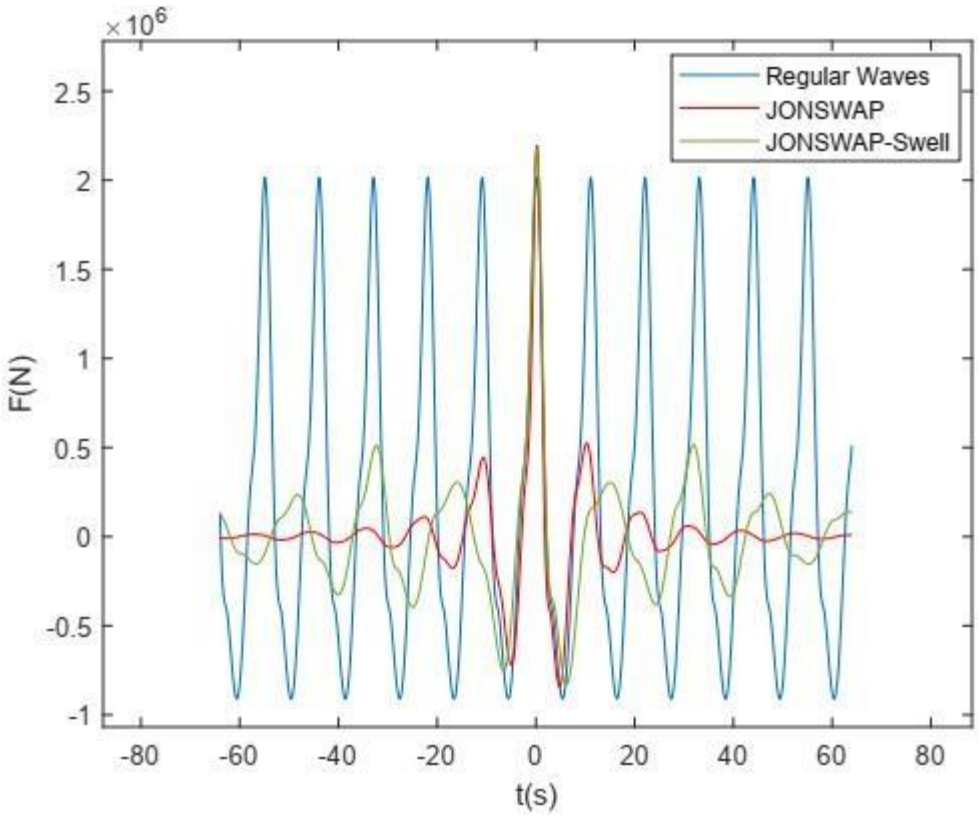

Figure 4.1: Comparison of total horizontal force-time history computed using different types of waves and their respective wave theory.

4.1. Total Horizontal Substructure Forces Using Different Types of Waves

Regular Waves (Stokes' 5th)

The total horizontal substructure force obtained from Stokes' 5th is the lowest among all types of waves, as shown in Figure 4.1 above. This is due to the deviation in the prediction of the water particle kinematics as portrayed in Figure 2.1. In Figure 2.1, it was shown that Stokes' 5th Order Wave Theory overpredicts the water particle kinematics at the substructural level while it underpredicts the water particle kinematics at the superstructural level. However, the maximum values of water particle kinematics occur at the wave crest and decrease exponentially with depth. As a result, the underprediction in the water particle kinematics at the superstructural level contributed more significantly to the underprediction of the total horizontal force compared to the overprediction that occurred in the substructural level, thus causing an overall underestimation of the

total horizontal substructure force. While the overdesign of the members at the substructural level might not indicate any serious engineering issue, the under-design of the members at the superstructural level, on the other hand, can be a problem because the forces at the superstructure level are more critical due to the water particle kinematics approaching their maximum values at the superstructural level. As mentioned earlier in Chapter 1, most of the existing offshore platforms are designed based on Stokes' 5th order wave theory, therefore the value of total horizontal substructure force obtained from Stokes' 5th order wave theory will serve as a reference value for the assessment on the sufficiency of the existing design.

Irregular Waves (2nd Order)

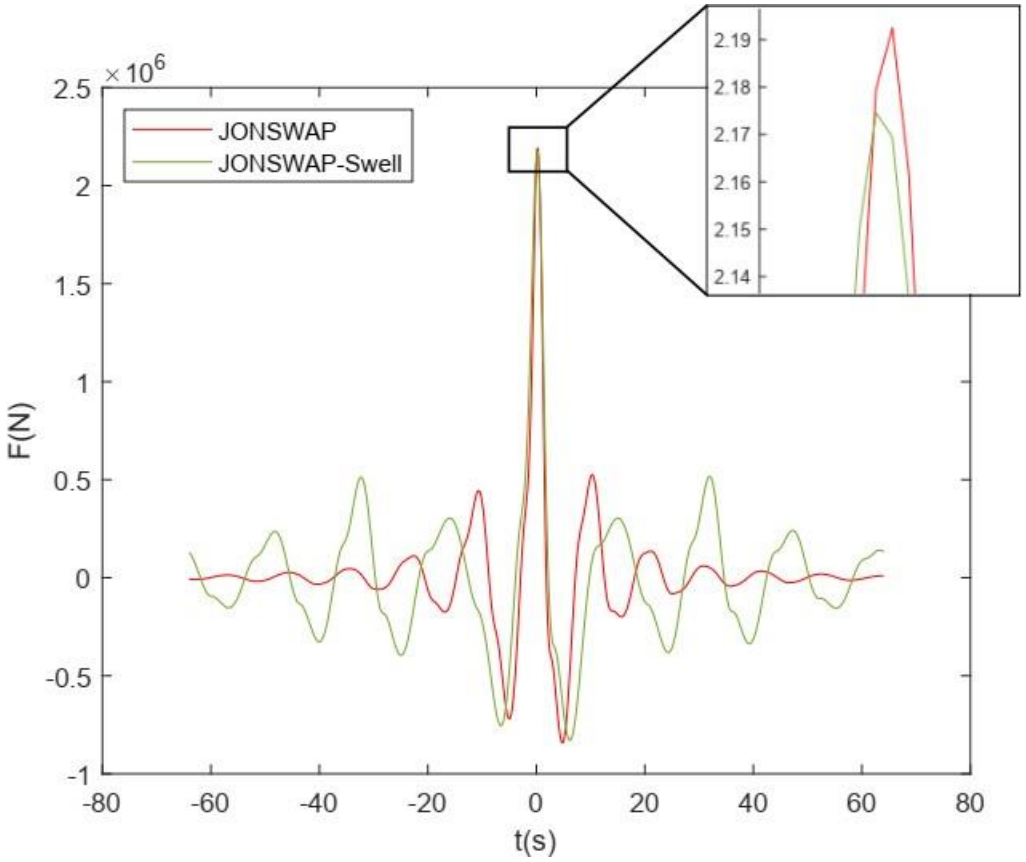

Figure 4.1.1: Total horizontal force-time history computed using 2nd order wave theory

To examine the effect of spectral shapes on the forces acting on the jacket structure, two different spectral shapes, JONSWAP spectrum and the observed spectral shape in Southern South China Sea (JONSWAP-Swell), were compared against each other. JONSWAP spectrum is one of the most widely used spectral shapes in the design of offshore platforms, therefore it is important to have another spectral shape compared against it in order to assess the sufficiency of the existing design. Since the subjects of this study are the offshore platforms in Malaysia, JONSWAP-Swell was adopted for the comparison against JONSWAP spectrum as it represents the sea state in this area more accurately. While JONSWAP spectrum is consisted only of wind waves, the observed spectral shape in Southern SCS can be fitted by adding a swell wave component of a different peak period to the wind wave, where the wind component is also represented by JONSWAP spectrum. In comparison to the Stokes' 5^{th} regular waves, both of these spectral shapes achieved a larger total horizontal substructure force with JONSWAP spectrum achieving a slightly larger total force compared to JONSWAP-Swell. The difference in the total force between the two spectral shapes is caused by the 2nd order terms in the water particle kinematics and the harmonics due to the interactions between the swell and wind components. In Figure 4.1.1, a rather interesting observation can be made where the total horizontal force-time history for JONSWAP spectrum decays steadily over time while the total horizontal force-time history for JONSWAP-Swell displays a spike at -32.3s and 32.3s, both of which exhibit a higher value of total horizontal force than the two peaks at -16s and 16s immediately adjacent to the highest peak. This is due to the constructive interference of the wave components which results in a larger amplitude, thus larger force. Although the swell wave component and wind wave component are summed up linearly to the same significant wave height (Hs) as JONSWAP spectrum, the additional swell component in JONSWAP-Swell has a different peak period, resulting in a periodic constructive interference with the wind wave component when the swell wave component is in phase with the wind wave component.

4.2. Effects of Directionality

In order to better represent the real sea state where waves propagate in different directions, the effect of directionality was incorporated by spreading the wave components normally by Gaussian distribution as discussed in Chapter 2. As opposed to unidirectional focused wave groups, when a wave group undergoes directional spreading, the energy density is reduced due the dissipation of energy into different directions, causing the energy to no longer be focused in the mean direction of wave propagation, thus reducing the total horizontal force on the substructure. Table 1 below summarises and compares the maximum total horizontal substructure forces by each spectral shape when they undergo directional spreading of 15º and 30º against their respective unidirectional counterparts.

Table 4.2.1: Maximum total horizontal substructure force in unidirectional and directional cases.

	Total Horizontal Substructure Force (MN)		
Spectral Shape	Unidirectional	Spectral Shape	
		15º spreading	30º spreading
JONSWAP	2.1924	2.1511	1.8859
JONSWAP-Swell	2.1752	2.1792	1.9581

When directionality was incorporated into the two spectral shapes, an overall reduction in the total forces was expected, though the forces did not observe a consistent trend of reduction across the board. With the degree of spreading set to 15º, the total horizontal substructure force for JONSWAP spectrum was reduced by roughly 0.19%. Interestingly, when directionality was incorporated in the observed spectral shape in Southern SCS, the structure experienced a slight increment of 0.18% in the total horizontal substructure force. To further investigate the effect of directionality, the degree of spreading was increased to 30º. As a result, the total horizontal force reduced by approximately 15% and 10% for JONSWAP spectrum and JONSWAP-Swell, respectively. In this case, both

spectral shapes observed a significant reduction in the total horizontal substructure force where the degree of reduction in the total horizontal force was higher in JONSWAP spectrum compared to that of the observed spectral shape in Southern SCS. The above observations made are due to the difference in the rate of decay in particle kinematics in terms of water level, which will be further explained in Section 4.4.

4.3. Horizontal Forces in Different Depth Regions

Particle kinematics can be described as a function which decreases exponentially along with the water level from wave crests to the seabed. Therefore, it is crucial to study the variation of the forces at different depth ranges and its contribution to the total horizontal force. As usual, Stokes' 5th Order Wave Theory will serve as a reference value for comparison since it is the most commonly adopted theory in practice. The two spectral shapes, both approximated based on 2nd Order Random Wave Theory, will be compared against each other in reference to the Stokes' 5th. In this examination, the total depth of 70m is divided into three different depth regions: crest to -10m, -10m to -40m and -40m to -70m. The force time history in each individual depth range is shown below in Figure 4.3.1, Figure 4.3.2 and Figure 4.3.3 respectively.

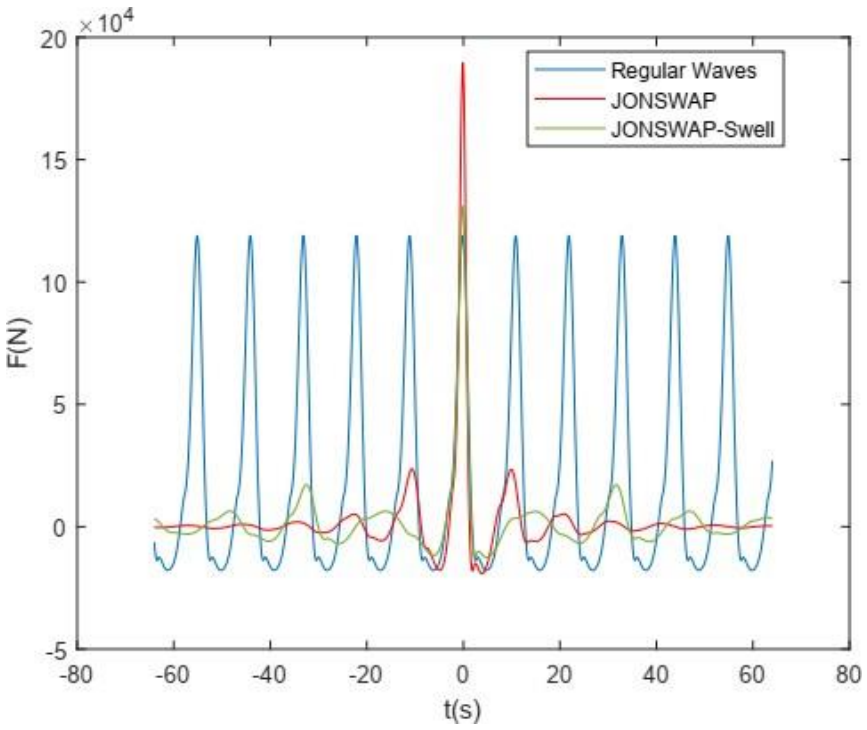

Figure 4.3.1: Horizontal force-time history using regular waves and irregular waves of different spectral shapes from crest to -10m.

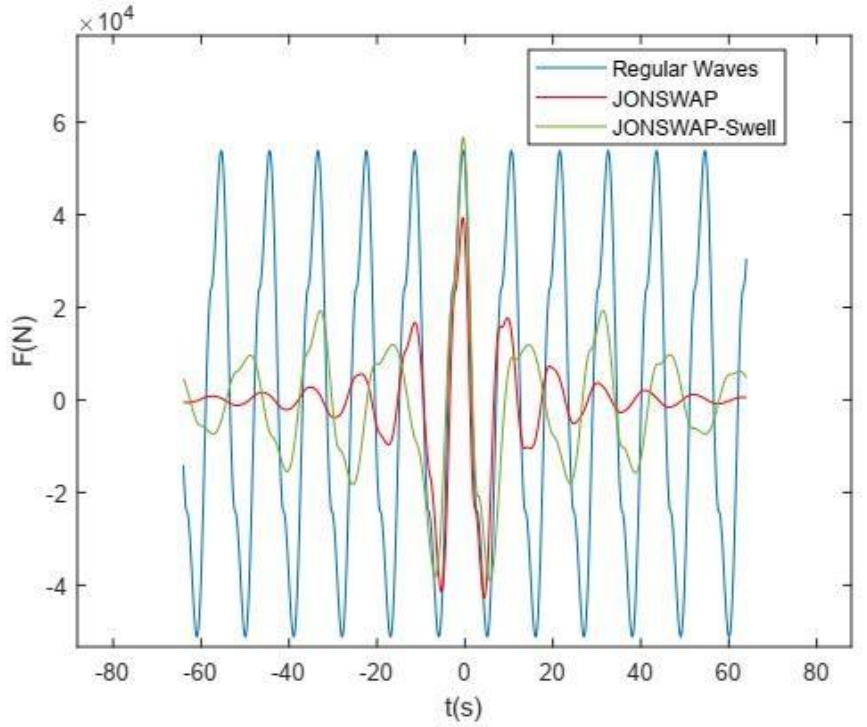

Figure 4.3.2: Horizontal force-time history using regular waves and irregular waves of different spectral shapes from -10m to -40m.

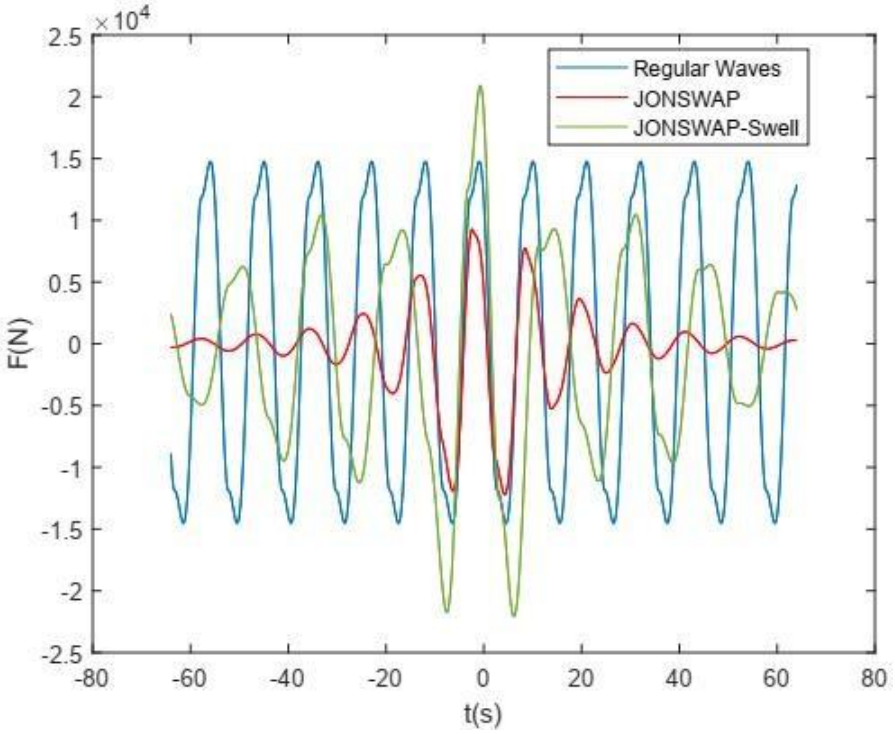

Figure 4.3.3: Horizontal force-time history using regular waves and irregular waves of different spectral shapes from -40m to -70m.

From the crest to the depth of -10m (Figure 4.2.3), the force generated by JONSWAP is the greatest, followed by JONSWAP-Swell, whereas the smallest force is recorded by Stokes' 5th. This is directly related to the tendency of Stokes' 5th to underestimate the particle kinematics above still water level while 2nd Order Wave Theory tends to do the opposite as portrayed in Figure 2.1. However, below still water level, Stokes' 5th tends to overestimate the particle kinematics while 2nd Order Random Wave Theory underestimates. This trend can be observed in both the depth range of -10m to -40m and -40m to -70m (Figure 4.2.4 and Figure 4.2.5, respectively) when JONSWAP spectrum was compared against regular waves (Stokes' 5th). In both of these depth ranges, JONSWAP spectrum gives a significantly smaller force in comparison to regular waves. On the other hand, JONSWAP-Swell yields the largest force in both depth ranges. This is due to the lower rate of particle kinematics decay in JONSWAP-Swell which will be discussed in the next section.

4.4. 2nd Order Particle Kinematics

Unidirectional Cases

In the previous section, it was shown that JONSWAP-Swell consistently gives higher forces in depth region below -10m. As mentioned previously, particle kinematics varies exponentially in terms of the water level. In 2nd Order Wave Theory, the particle kinematics are made up of a few components. These components are the difference term, the linear term, the summation term and the Stokes' 2nd Order term. Therefore, to further examine this phenomenon, it is necessary to obtain the different components of particle kinematics at different water levels. A comparison was then made between the components from JONSWAP and JONSWAP-Swell to understand such occurrence. Figure 4.4.1 below shows the variation each component of particle kinematics from the two spectral shapes at different water levels from crest to the seabed. Interestingly, similar trend occurs in terms of time as well. In Figure 4.1.1, it was shown that the total horizontal force decays at a slower rate in JONSWAP-Swell in comparison to JONSWAP. Upon the basis we worked on in Chapter 2, particle kinematics can be derived from the surface elevation function with Laplace equation, which indicates that particle kinematics depend on the surface elevation as well. The 2nd order surface elevation-time history was plotted and shown below in Figure 4.4.2.

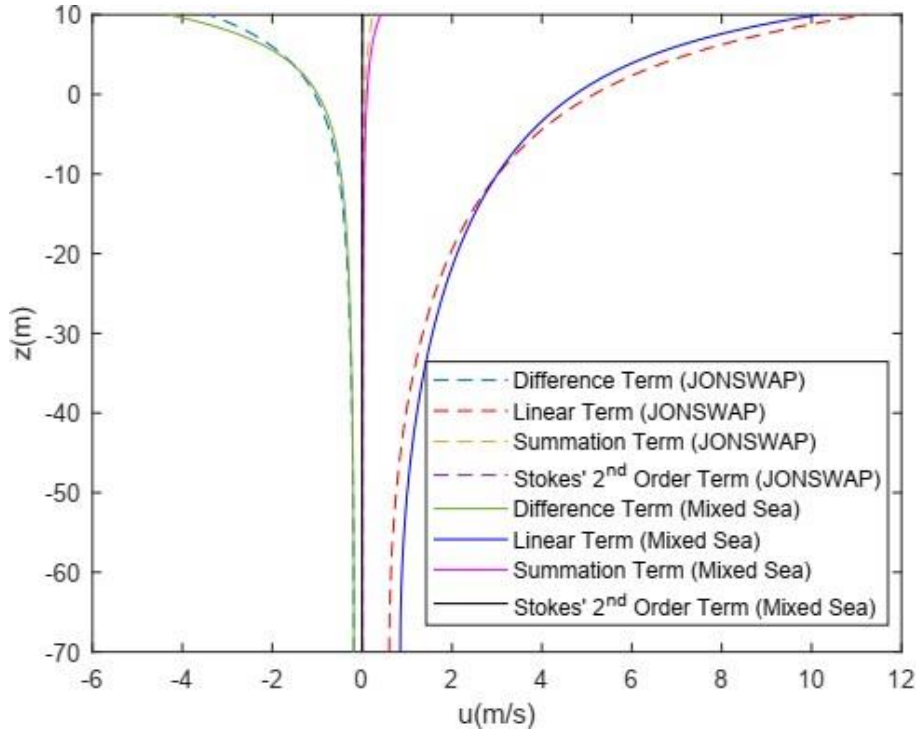

Figure 4.4.1: Particle Kinematics Components of 2nd Order Random Wave Theory.

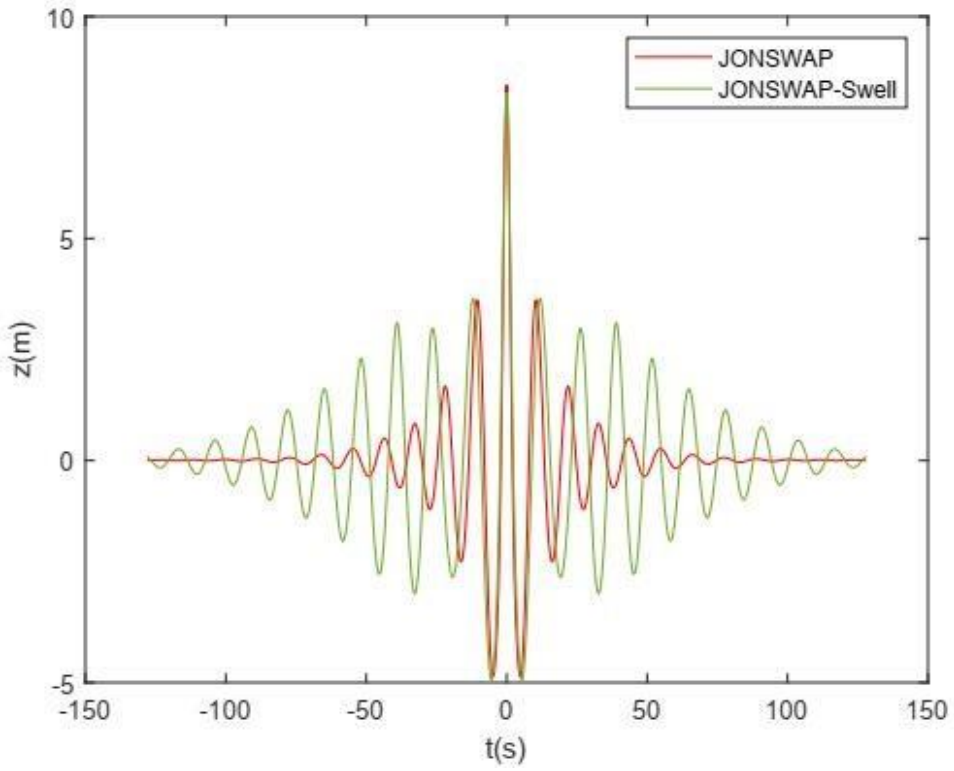

Figure 4.4.2: Comparison of 2nd Order Surface Elevations Between Two Spectral Shapes.

As one can observe in Figure 4.4.1, the difference term is much larger in JONSWAP-Swell, resulting in an overall lower value of 2nd order wave particle kinematics which yields the slightly lower maximum total horizontal force above still water level. Besides, Figure 4.4.1 shows that the linear term in 2nd order water particle kinematics for mixed sea decays much slower than that of JONSWAP spectrum in terms of depth. At water levels below -10m, the linear term of JONSWAP-Swell becomes larger than that of JONSWAP. Therefore, the horizontal forces from JONSWAP in this depth region are smaller compared to JONSWAP-Swell. In Figure 4.4.2, we can observe that despite the lower maximum surface elevation, JONSWAP-Swell displays significantly higher surface elevation as the waves decay in terms of time. This shows that JONSWAP-Swell is more broad-banded compared to JONSWAP as more wave components in JONSWAP-Swell have higher energy. As a result, wave particle kinematics in JONSWAP-Swell can maintain a higher value over a longer period of time, which explains the slower decay in its total horizontal force-time history.

Directional Cases

In Section 4.2, it was observed that when the directional spreading was set to 15º, the total horizontal force for JONSWAP reduced by 0.19% while JONSWAP-Swell experienced in slight increment of 0.18% in the total horizontal force. However, the force was expected to reduce when directionality was incorporated. Since force is closely related to the particle kinematics, the difference term of particle kinematics in the unidirectional and directional cases for both spectral shapes were plotted and compared against each other in Figure 4.4.3 below. Note that the values of 2^{nd} Order Stokes' Term in directional cases have the order of magnitude of 10^{-3}, therefore they are insignificant to the overall particle kinematics, thus not plotted for comparison.

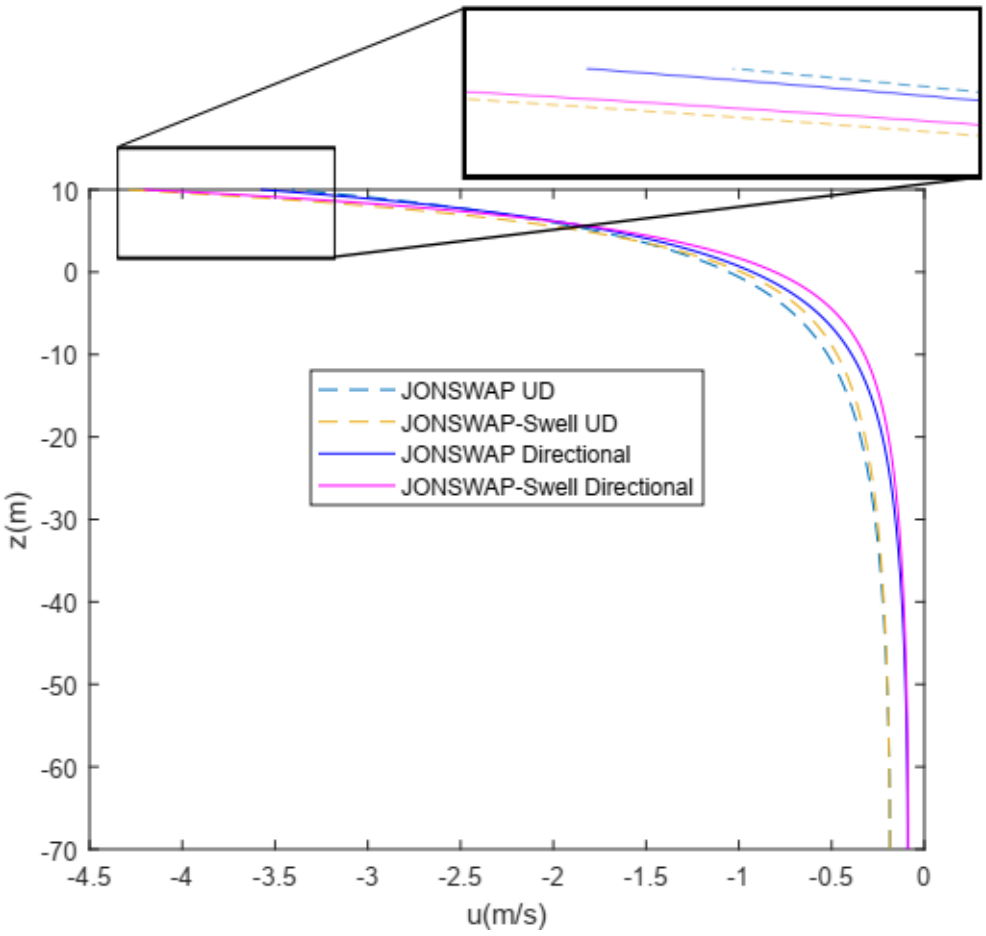

Figure 4.4.3: Comparison of Difference Term in Particle Velocity Between Unidirectional and Directional (15º) cases of Two Spectral Shapes.

As we can see in Figure 4.4.3, from the crest to the seabed, the difference term in the particle kinematics of directional JONSWAP-Swell is consistently smaller than the difference term in unidirectional JONSWAP-Swell. This causes the particle kinematics to be slightly higher at the superstructure level and owing to the nature of 2nd Order Random Wave Theory to overestimate forces above still water level, the total horizontal force increases slightly. On the other hand, for directional JONSWAP, the difference term is larger at the superstructure level compared to that of unidirectional JONSWAP. Since the particle kinematics are at the highest above still water level, it leads to an overall lower particle kinematics compared to the unidirectional case and ultimately reducing the total horizontal force.

Additionally, in the case where the directional spreading is set to 30º, JONSWAP-Swell observes a smaller degree of reduction at 10% compared to 15% reduction in JONSWAP. Similarly, in order to find out why the degree of reduction was different, the 2nd Order particle kinematics in unidirectional and directional cases for both spectral shapes were plotted and compared against each other in Figure 4.3.4 below.

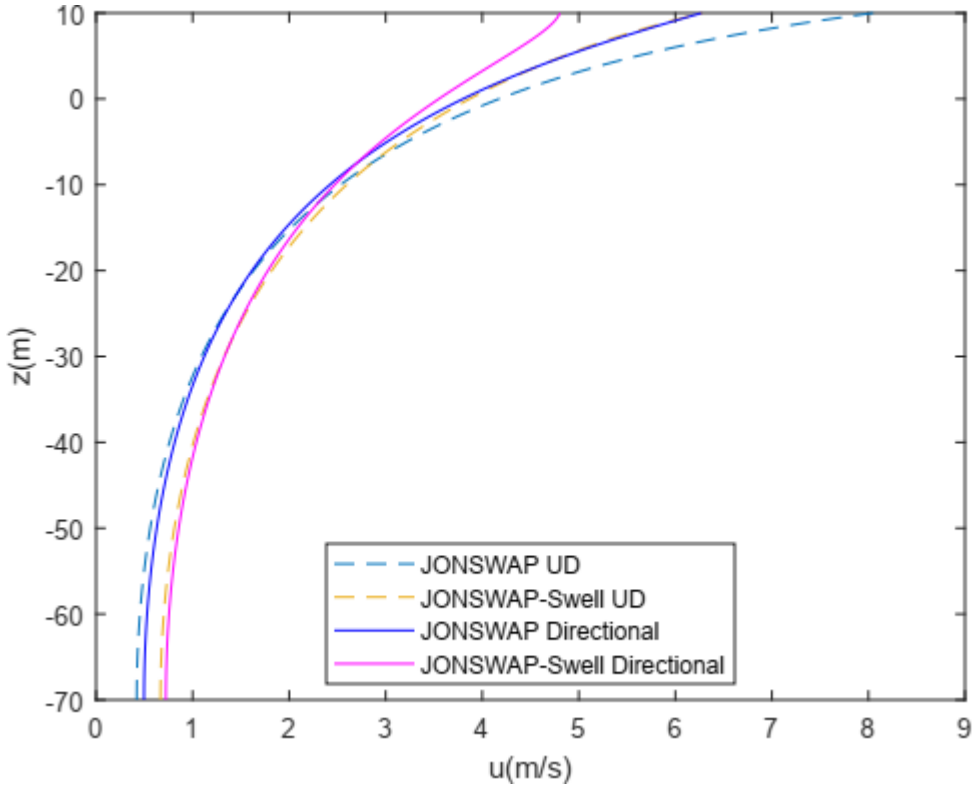

Figure 4.4.4: Comparison of 2nd Order Particle Velocity Between Unidirectional and Directional (30º) cases of Two Spectral Shapes.

In Figure 4.4.4 above, it is shown that the degree of reduction in particle kinematics of JONSWAP-Swell is much smaller than that of JONSWAP. As discussed several times in the above sections, the forces are directly related to the particle kinematics, therefore a smaller degree of reduction in the particle kinematics for JONSWAP-Swell directly leads to the observed smaller degree of reduction in the total horizontal force compared to JONSWAP.

5. CONCLUSION AND RECOMMENDATION

The total horizontal substructure force obtained using Stokes' 5th Order Wave Theory is lower than that of each spectral shape computed based on 2nd Order Random Wave Theory, albeit not by much. Since the values are in the same order of magnitude with a deviation of less than 10%, they are said to be similar to each other. As 2nd Order Random Wave Theory provides a more accurate representation of the real sea states, it is deduced that the jacket structures designed based on Stokes' 5th Order Wave Theory are sufficient to resist the base shear. However, after a further examination in the forces in different depth regions, it is discovered that the forces generated by Stokes' 5th Order Wave Theory above the still water level are lower compared to using 2nd Order Random Wave Theory. Besides, below the still water level, Stokes' 5th Order Wave Theory gives higher forces compared to 2nd Order Random Wave Theory. This shows that jacket structures designed based on Stokes' 5th may have overdesigned members in the substructural level while the members in the superstructural level may be under-designed.

Among the two spectral shapes adopted, JONSWAP yields a larger maximum total horizontal force but the force decays quickly after the peak. While JONSWAP-Swell produces a slightly lower peak in the total horizontal force, the force is sustained over a longer duration after reaching the peak. This is due to the energy band of JONSWAP-Swell being much broader than that of JONSWAP, causing energy to be more widely spread over the time domain, resulting in a lower rate of decay in the surface elevation in terms of time. A further investigation shows that JONSWAP-Swell also exhibits a much higher horizontal force compared to JONSWAP in depth regions below the still water level. However, the horizontal force by JONSWAP-Swell is much lower in comparison to JONSWAP above still water level. This is due to the lower rate of decay in different terms of 2nd Order particle kinematics in the depth domain which results in the higher particle kinematics below the still water level. This shows that jacket structures in Malaysia designed based on JONSWAP spectrum may have overdesigned members in the upper elevation while the members in the lower elevation may be significantly under-designed.

When directionality was incorporated in the force computation, the total force will not necessarily reduce as observed in JONSWAP-Swell with 15º of directional spreading. However, the increment is rather insignificant at 0.18% more than the total force of unidirectional JONSWAP-Swell. For 15º directionally spread JONSWAP, the total horizontal force is reduced by a mere 0.19%. On the other hand, when both spectral shapes are directionally spread by 30º, the total horizontal forces of both JONSWAP and JONSWAP-Swell record a significant reduction at 15% and 10%, respectively. Since the directional spreading in Southern South China Sea ranges from 10º to 15º, it is safe to say that the effect of directionality is insignificant and can be neglected in the design.

When the total horizontal substructure was computed, the effect of current was not considered, which can result in either a large increase in the total horizontal force if the current is co-flowing with the wave and or a large reduction if the current direction opposite to the direction of wave propagation. According to Latheef et al. (2018), the interaction between wave and current can change the behaviour of the wave and may also cause amplifications of the wave. When wave current interactions are included, the truncation order required to accurately predict the waves also increases. In other words, the present design practice may not be predicting the waves accurately which could lead to overestimation or underestimation of the loadings acting on the structure. Considering how 2nd Order Random Wave Theory produces so many surprising results, a fully nonlinear wave modelling based on a method known as Boundary Element Modelling introduced by Hague and Swan (2009) should be implemented for a higher accuracy. Besides, the force computation was based on the assumption of no wave-in-deck (WID) loading throughout the platform service life. WID loading is a lateral load acting on the structure when the wave crest reaches enough height to hit the topside of the structure, resulting in a rapid transfer of momentum from the fluid to the rigid deck. However, in reality, offshore platforms inevitably experience settlement in the foundation, thus causing the airgap to reduce over time. In the worst-case scenario, the airgap intended to prevent waves from hitting the deck will no longer exist. Without the airgap, the wave crest will be able to reach the deck and cause WID load. Combined with the higher order wave theories and the effect of

current, WID loading on the structure can contribute significantly to the total horizontal force on the structure. WID loadings are most commonly computed based on momentum-flux formulation proposed by Graaf et al. In this method, the deck is assumed to have zero porosity and momentum is dissipated instantaneously. Due to these assumptions, the result obtained is more conservative as a large amount of momentum is transferred from the fluid to the deck over a short duration. Fortunately, Ma and Swan (2020) recently published a new method for the computation of WID loading. This new method is known as Lagrangian Momentum Absorption (LMA). Rather than taking a 'global approach', LMA method adopts a 'component approach' by using the Lagrangian scheme to track the momentum transfer of each individual component. Through this method, the porosity of the deck is considered, and the momentum is dissipated progressively based on the interaction of waves with parts of the deck. This makes the LMA method capable of providing a more accurate prediction of the WID loads, thus this method should be implemented as the WID load model in the further works. In the current model, the structure is assumed to react statically to the forces. For irregular waves of broad-banded spectral shapes, including the dynamic response can lead to more enhanced loads.

REFERENCES

Amurol Jamal S, Ewans K, Sheikh R et al. (2014). Measured wave spectra offshore Sabah & Sarawak, Malaysia. *In: Offshore Technology Conference-Asia.* Offshore Technology Conference.

Boccotti, P. (1989). On Mechanics of Irregular Gravity Waves. *Atti Accademia Nazionale dei Lincei, Memoire VIII 19*, 111-170.

Cassidy, M. J., Taylor, P. H., Taylor, R. E. & Houlsby, G. T. (2002). Evaluation of longterm extreme response statistics off jack-up platforms. *Ocean Engineering 29(13)*, pp. 1603-1631.

Dean, R.G. and Dalrymple, R.A. (1991). *Water Wave Mechanics for Engineers and Scientists, Volume 2 of Advanced Series in Ocean Engineering.* World Scientific Publishing Co.

Feng, X., Taylor, P. H., Dai, S., Day, A. H., Willden, R. H. J. & Adcock, T. A. A. (2020). Experimental investigation of higher harmonic wave loads and moments on a vertical cylinder by a phase-manipulation method. *Coastal Engineering 160*.

Fenton, J. D. (1985). A Fifth-Order Stokes Theory for Steady Waves. *Journal of Waterway, Port, Coastal and Ocean Engineering 111*, 216.

Gibson, R. S. & Swan, C. (2007). The evolution of large ocean waves: the role of local and rapid spectral changes. *Proceedings of the Royal Society A: Mathematical, Physical and Engineering Science 463*, pp. 21-48.

Goda, Y. (2000). *Random Seas and Design of Maritime Structures, Volume 15 of Advanced Series in Ocean Engineering.* World Scientific Publishing Co.

Graaf, J. W. v. d., Tromans, P. S., Vanderschuren, L. (1995). Wave Loads on Decks. *Shell Offshore Struct. Eng. Newsl. (10)*.

Hague, C. & Swan, C. (2009). A multiple flux boundary element method applied to the description of surface water waves. *Journal of Computational Physics 228(14)*, pp. 5111-5128.

ISO 19901-1 Petroleum and natural gas industries-specific requirements for offshore structures-part 1: metocean design and operating conditions. (2005). *ISO*.

Johannessen, T. B. & Swan, C. (2001). A laboratory study of the focusing of transient and directionally spread surface water waves. *Proceedings of the Royal Society of London. Series A: Mathematical, Physical and Engineering Sciences 457(2008)*, pp. 971-1006.

Johannessen, T. B. & Swan, C. (2003). On the nonlinear dynamics of wave groups produced by the focusing of surface-water waves. *Proceedings of the Royal Society of London. Series A: Mathematical, Physical and Engineering Sciences 459(2032)*, pp. 1021-1052.

Kaplan, P., Murray, J. J., Yu, W. C. (1995). Theoretical analysis of wave impact forces on platform deck structures. *n: OMAE 1995, 14th International Conference on Offshore Mechanics & Arctic Engineering, vol. 1* (p. 189). Copenhagen, Denmark: ASME.

Latheef, M. & Swan, C. (2013). A laboratory study of wave crest statistics and the role of directional spreading. *Proceedings of the Royal Society of London. Series A: Mathematical, Physical and Engineering Sciences 469: 20120696(2013)*.

Latheef, M. (2014). Surface wave statistics in directionally spread seas. *PhD thesis, Imperial College London*.

Latheef, M., Abdulla, N., & Jupri, M.F.M. (2018). Wave current interaction: Effect on force prediction for fixed off-shore structures. *MATEC Web of Conferences, 203*. doi:https://doi.org/10.1051/matecconf/201820301011

Longuet-Higgins, M. S. & Stewart, R. W. (1960). Changes in the form of short gravity waves on long waves and tidal currents. *Journal of Fluid Mechanics 8(4),*, pp. 565-583.

Ma, L., Swan, C. (2019). An experimental study of wave-in-deck loading and its dependence on the properties of the incident waves. *Journal of Fluids and Structures,*. doi:https://doi.org/10.1016/j.jfluidstructs.2019.102784

Ma, L., Swan, C. (2020). The effective prediction of wave-in-deck loads. *Journal of Fluids nd Structures, 95*. doi:https://doi.org/10.1016/j.jfluidstructs.2020.102987

Morison, J. R., O'Brien, M. P., Johnson, J. W. & Schaaf, S. A. (1950). The force exerted by surface waves on piles. *Journal of Petroleum Technology 2, 149.*

PTS 34.19.10.30 Petronas technical standards: Design of fixed offshore structures (working stress design). (2012). *PTS*.

Sharma, J. N. & Dean, R. G. (1981). Second-order directional seas and associated wave forces. *Society of Petroleum Engineers journal 21(1)*, pp. 129-140.

Swan, C., Latheef, M., Ma, L. (2016). The loading and reliability of fixed steel structures in extreme seas: recent advances and required improvements. *The 3rd Offshore Structural Reliability Conference*.

Tromans, P. S., Anaturk, A. & Hagemeijer, P. (1991). A new model for the kinematics of large ocean waves – applications as a design wave. *In Proceedings of 1st Offshore and Polar Engineering Conference (ISOPE)*, pp. 64-71.

APPENDICES

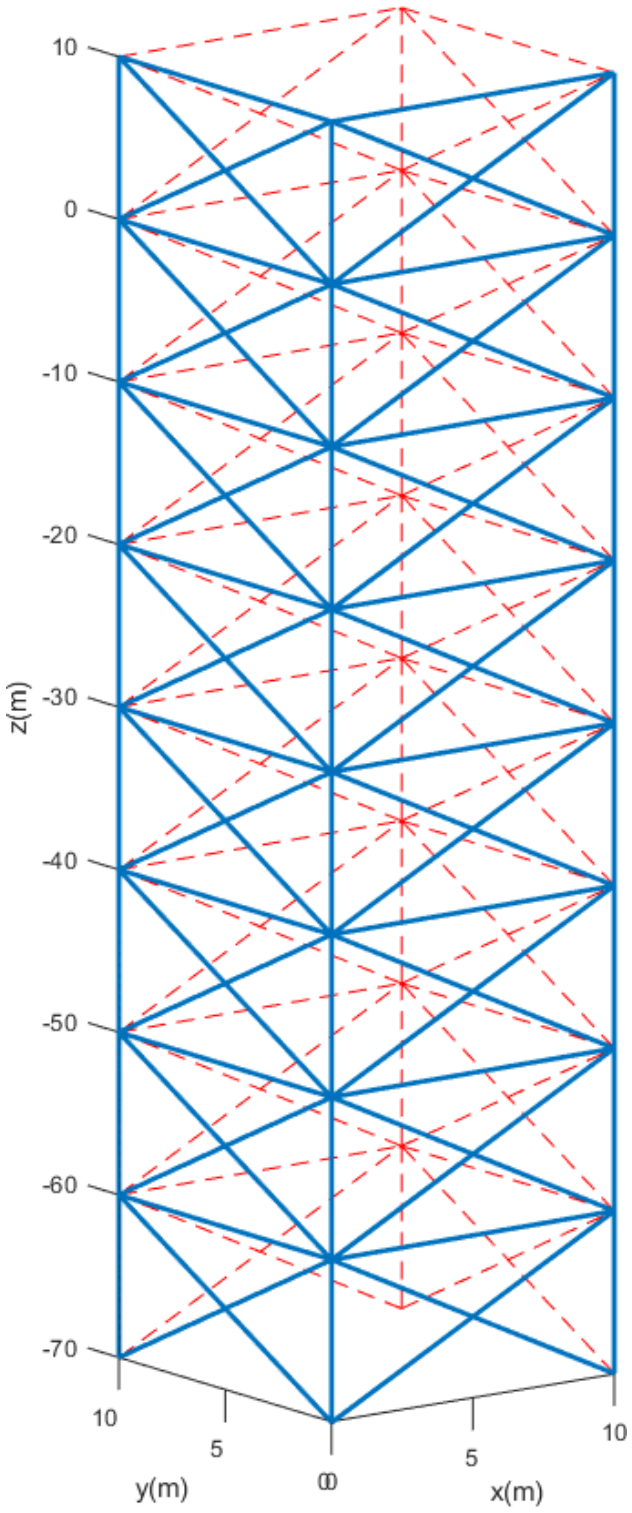

Appendix 1: 3D view of jacket structure model.

Appendix 2: Manual calculations of horizontal substructure force for code verification

Column located at trough (C1)

Drag Coefficient, $C_d = 1$

Inertia Coefficient, $C_m = 1$

Density of fluid, $\rho = 1025 kg/m^3$

Water depth = 70m

Wave Amplitude, a = 7.5m

Wave Period, T = 11s

Circular Frequency, $\omega = 0.571$ rad/s

Wave Number, $k = 0.0338 m^{-1}$

Time, t = 0

Spatial Location, x = 46.473m (approximate location of wave trough)

Column spans from seabed (-70m) to 10m above still water level, however, since waves will only reach -7.5m max, the z considered will only be up till that elevation (70 - 7.5 = 62.5m).

$$u^2 = \frac{a^2\omega^2 cosh^2(kz) sin^2(\omega t - kx)}{sinh^2(kd)}$$

$$u^2 = \frac{7.5^2 \times 0.571^2 cosh^2(0.0338 \times z) sin^2(0.571 \times 0 - 0.0338 \times 46.473)}{sinh^2(0.0338 \times 70)}$$

$$u^2 = 0.658 cosh^2(0.0338z) m^2 s^{-2}$$

$$\frac{du}{dt} = \frac{a\omega^2 cosh(kz) cos(\omega t - kx)}{sinh(kd)}$$

$$\frac{du}{dt} = \frac{7.5 \times 0.571^2 cosh(0.0338 \times z) cos(0.571 \times 0 - 0.0338 \times 46.473)}{sinh(0.0338 \times 70)}$$

$$\frac{du}{dt} = 4.134 \times 10^{-6} cosh(0.0038z)$$

$$F_x = C_d \frac{1}{2} \rho D \int_{z=0}^{z=62.5} u^2 dz + C_m \rho \frac{\pi D^2}{4} \int_{z=0}^{z=62.5} \frac{du}{dt} dz$$

Substituting the formerly calculated u^2 and $\frac{du}{dt}$ into the above equation,

$F_x = 1 * 0.5 * 1025 * 1 * 186.91 + 1 * 1025 * 0.785 * 4.982 * 10^{-4}$

= 95791.77 N

= 9.5791 x 10^4 N

Column located at crest (C2)

Drag Coefficient, $C_d = 1$

Inertia Coefficient, $C_m = 1$

Density of fluid, $\rho = 1025 kg/m^3$

Water depth = 70m

Wave Amplitude, a = 7.5m

Wave Period, T = 11s

Circular Frequency, $\omega = 0.571$ rad/s

Wave Number, $k = 0.0338 m^{-1}$

Time, t = 0

Spatial Location, x = 139.4195m (approximate location of wave crest)

Column spans from seabed (-70m) to 10m above still water level, however, since waves will only reach 7.5m max, the z considered will only be up till that elevation (70 + 7.5 = 77.5m).

$$u^2 = \frac{a^2\omega^2 cosh^2(kz) sin^2(\omega t - kx)}{sinh^2(kd)}$$

$$u^2 = \frac{7.5^2 \times 0.571^2 cosh^2(0.0338 \times z) sin^2(0.571 \times 0 - 0.0338 \times 139.4195)}{sinh^2(0.0338 \times 70)}$$

$$u^2 = 0.658 cosh^2(0.0338z) m^2 s^{-2}$$

$$\frac{du}{dt} = \frac{a\omega^2 cosh(kz) cos(\omega t - kx)}{sinh(kd)}$$

$$\frac{du}{dt} = \frac{7.5 \times 0.571^2 cosh(0.0338 \times z) cos(0.571 \times 0 - 0.0338 \times 139.4195)}{sinh(0.0338 \times 70)}$$

$$\frac{du}{dt} = 4.576 \times 10^{-6} cosh(0.0038z)$$

$$F_x = C_d \frac{1}{2} \rho D \int_{z=0}^{z=77.5} u^2 dz + C_m \rho \frac{\pi D^2}{4} \int_{z=0}^{z=77.5} \frac{du}{dt} dz$$

Substituting the formerly calculated u^2 and $\frac{du}{dt}$ into the above equation,

$F_x = 1 * 0.5 * 1025 * 1 * 484.14 + 1 * 1025 * 0.785 * 9.244 * 10^{-4}$

= 248122.49 N

= 2.4812×10^5 N

Column located at trough (C3)

Drag Coefficient, $C_d = 1$

Inertia Coefficient, $C_m = 1$

Density of fluid, $\rho = 1025 kg/m^3$

Water depth = 70m

Wave Amplitude, a = 7.5m

Wave Period, T = 11s

Circular Frequency, $\omega = 0.571$ rad/s

Wave Number, $k = 0.0338 m^{-1}$

Time, t = 0

Spatial Location, x = 46.473m (approximate location of wave crest)

Column spans from seabed (-70m) to 20m below still water level (-20m). It is fully submerged, the z considered will only be from the bottom to the top of the column.

$$u^2 = \frac{a^2\omega^2 cosh^2(kz) sin^2(\omega t - kx)}{sinh^2(kd)}$$

$$u^2 = \frac{7.5^2 \times 0.571^2 cosh^2(0.0338 \times z) sin^2(0.571 \times 0 - 0.0338 \times 46.473)}{sinh^2(0.0338 \times 70)}$$

$$u^2 = 0.658 cosh^2(0.0338z) m^2 s^{-2}$$

$$\frac{du}{dt} = \frac{a\omega^2 cosh(kz) cos(\omega t - kx)}{sinh(kd)}$$

$$\frac{du}{dt} = \frac{7.5 \times 0.571^2 cosh(0.0338 \times z) cos(0.571 \times 0 - 0.0338 \times 46.473)}{sinh(0.0338 \times 70)}$$

$$\frac{du}{dt} = 4.134 \times 10^{-6} cosh(0.0038z)$$

$$F_x = C_d \frac{1}{2} \rho D \int_{z=0}^{z=50} u^2 dz + C_m \rho \frac{\pi D^2}{4} \int_{z=0}^{z=50} \frac{du}{dt} dz$$

Substituting the formerly calculated u^2 and $\frac{du}{dt}$ into the above equation,

$F_x = 1 * 0.5 * 1025 * 1 * 87.838 + 1 * 1025 * 0.785 * 3.201 * 10^{-4}$

= <u>45017.23 N</u>

= <u>4.5017 x 10^4 N</u>